Physicochem. Probl. Miner. Process. 53(1), 2017, 17−33

www.minproc.pwr.wroc.pl/journal/

Physicochemical Problems of Mineral Processing

ISSN 1643–1049 (print)
ISSN 2084–4735 (online)

Received August 27, 2015; reviewed; accepted December 19, 2015

A STUDY OF BUBBLE-PARTICLE INTERACTIONS IN A COLUMN FLOTATION PROCESS

Gan CHENG[*], Changliang SHI[*], Xiaokang YAN[**], Zhijun ZHANG[***], Hongxiang XU[***], Yang LU[*]

* School of Materials Science and Engineering, Henan Polytechnic University, Jiaozuo 454000, Henan, China, chenggan464@126.com

** School of Chemical Engineering and Technology, China University of Mining and Technology, Xuzhou 221116 Jiangsu, China

*** School of Chemical and Environmental Engineering, University of Mining and Technology (Beijing), Beijing 100083, China

Abstract: Bubble-particle interactions play an important role in flotation. This study examines the behaviour of bubble clusters in a turbulent flotation cell. Particularly, the bubble-particle interaction characteristics in flotation are investigated. The bubble size in a flotation column was measured using an Olympus i-SPEED 3 high-speed camera. Relationships between the circulating volume, bubble size and bubble terminal velocity were discussed. Probabilities of collision, attachment, detachment and acquisition between bubbles and particles in different circulating volumes were calculated based on the flotation kinetic theory. Using the extended Derjaguin–Landau–Verwey–Overbeek (EDLVO) theory, the relationship between the potential energy and distance in bubble-particle interaction was analysed. The results demonstrated that as the circulating volume increased, the bubble size and velocity decreased. When the circulating volume increased from 0.253 to 0.495 m^3/h, the bubble diameter decreased from 511 to 462 μm, and the corresponding bubble velocity decreased from 43.1 to 37.5 mm/s. When the circulating volume remained constant as the particle size increased, probabilities of collision, attachment, detachment and acquisition increased. When the particle size remained constant as the circulating volume increased, these probabilities also increased. At a constant circulating volume as the particle size increased, the absolute value of the total potential energy between the particle and bubble increased. When the distance between the bubble and particle was 30 nm, the energy barrier appeared.

Keywords: *particle, bubble , column flotation, collision, attachment, detachment*

Introduction

Bubble-particle interactions are a central issue of flotation. They control the selectivity and efficiency of the process (Basaova and Hubicka, 2014). Generally, flotation

http://dx.doi.org/10.5277/ppmp170102

consists of three major sub-processes, that is collision, attachment and detachment. The probability of particle collection (P) by a bubble can be represented as follows:

$$P = P_c \cdot P_a \cdot (1 - P_d) \tag{1}$$

where P_c is the probability of collision between bubbles and particles, P_a probability of adhesion after collision and P_d probability that the subsequent detachment occurs.

Mineral flotation is a size-dependent process. Thus, fine, intermediate and coarse particles show different flotation behaviours (Fosu et al., 2015). There are many excellent reviews on the bubble-particle collision sub-process (Dai et al., 2000; Ralston et al., 2002). The attachment involves three elementary steps: (1) the thinning of the intervening water film between a bubble and a particle until film rupture occurs, (2) the rupture of the intervening liquid film and formation of a three-phase contact, and (3) expansion and relaxation of the three-phase contact line from the critical radius to form a stable wetting perimeter. Many investigators also studied the attachment sub-process (Nguyen and Schulze, 2004; Nguyen and Evans, 2004). As the bubble rise to the flotation froth by external forces in a flotation cell, the detachment causes removal of the attached particles from the bubble surface (Firouzi et al., 2011).

Ragab and Fayed (2012) developed a multiphase computational fluid dynamics (CFD) model by utilising the local turbulent energy dissipation and gas hold-up values, in conjunction with particle specific gravities, liquid surface tensions and contact angle parameters, to estimate the local pulp recovery rate. The model responses also suggested that the fine particle flotation kinetics was enhanced with increasing energy dissipation. Hence, it was proposed that the detachment sub-process affected the coarse particle recovery.

Pyke et al. (2004) derived the relationship between the flotation rate constant and collision, attachment and detachment probabilities of the bubble-particle:

$$K = \frac{Z_{pb}}{N_P} P_c \cdot P_a \left(1 - P_d\right). \tag{2}$$

The relationship is also described as follows (Mao, 1998):

$$k = \frac{3Q_g}{4\pi R_b^3} P = \frac{3J_g}{4R_b} P \tag{3}$$

.

Since Boutin and Tremblay invented the flotation column in the early 1960s, a column flotation technique has rapidly developed (Zhang et al., 2013). This work aims to study the interaction between the particle and bubble in the flotation column.

Models for bubble-particle interactions

Bubble-Particle Collision

Emerson (2007) used numerical solutions of the Navier-Stokes equations to derive the following relationship:

$$P_c = A\left(\frac{d_p}{d_b}\right)^n \tag{4a}$$

where d_p are d_b are diameters of particle and bubble respectively, A and n are parameters which are related to the Reynolds number.

Equation (4) indicates a power law relationship between the ratio of particle and bubble size and probability of collision with coefficients A and n. It also indicates that the collision is a function of the flow behaviour of particle and bubble, e.g., the Reynolds number of the bubble, $\mathrm{Re_b}$. Weber and Paddock (1988) used the power law relationship and numerical methods to derive expressions for A and for n as follows:

$$A = \frac{3}{2}\left(1+\frac{(3/16)\,\mathrm{Re}_b}{1+0.29\,\mathrm{Re}_b{}^{0.56}}\right) \tag{5}$$

$$n = 2 \tag{6}$$

where the Reynolds number Re_b is expressed as follows:

$$\mathrm{Re}_b = \frac{u_b d_b}{v} \tag{7}$$

where v is the kinematic viscosity in m^2/s. The kinematic viscosity for water is $1.005\cdot10^{-6}$ m^2/s.

Thus, the probability of collision P_c is described as follows:

$$P_c = \frac{3}{2}\left(1+\frac{(3/16)\,\mathrm{Re}_b}{1+0.29\,\mathrm{Re}_b{}^{0.56}}\right)\left(\frac{d_p}{d_b}\right)^2 \tag{4b}$$

This was the first collision model to be applied to wide ranges of particle and bubble sizes.

When an isolated bubble rises through a suspension of particles in a quiescent environment (Yoon and Luttrell, 1989) (Fig. 1), a flow pattern represented by an infinite series of streamlines develops. The arrangement of the streamlines depends on the fluids properties involved and geometry of obstacle placed in the flow field. It is

conceivable that small particles having negligible inertial force will follow the streamline, while large particles will deviate from it.

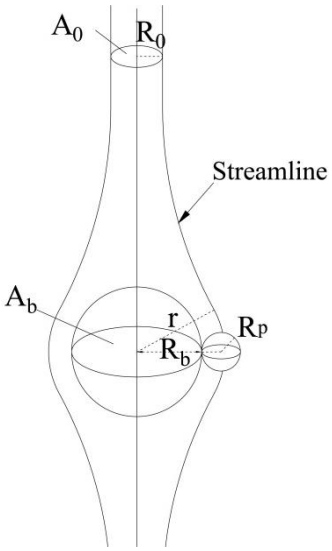

Fig. 1. Polar coordinate system describing the trajectory of a particle moving past a bubble

The trajectory of a particle is determined by the streamline that passes through its centre. It is assumed that the particles located in the path of the bubble and within the limiting radius (R_0) will collide with the bubble. Particles that lie outside this area will sweep past the bubble without having an opportunity for encounter. The probability of collision, which is defined as the fraction of particles in the path of bubble that actually collide with it, is determined by the ratio of area (A_0) inscribed by the limiting radius (R_0) to the area (A_b) inscribed by the bubble radius (R_b). Thus, the probability of collision (P_c) is given as follows:

$$P_c = \frac{A_0}{A_b} = \left(\frac{R_0}{R_b} \right)^2 . \tag{8}$$

The value of R_0 is unknown and must be determined from the mathematical description of the grazing streamline. When the Reynolds numbers of the bubble are different, then the trajectories formed by the bubble movements are also different.

For cases in which the Reynolds number is considerably less than unity, the streamlines are described by the well-known Stokes stream function. The probability of collision under Stokes flow conditions is described as follows:

$$P_c = \frac{3}{2}\left(\frac{R_p}{R_b}\right)^2 . \tag{9}$$

Under intermediate flow conditions the range of Reynolds numbers encountered for the sizes of bubbles typically employed during flotation range from 0.2 to 100. The probability of collision can be shown as follows:

$$P_c = \left(\frac{3}{2} + \frac{4\mathrm{Re}_b^{0.72}}{15}\right)\left(\frac{R_p}{R_b}\right)^2 . \tag{10}$$

For the potential flow conditions (involving very large Reynolds numbers), P_c can be obtained as follows:

$$P_c = 3\left(\frac{R_p}{R_b}\right) . \tag{11}$$

Bubble-particle attachment

Bubble-particle attachment depends on the particle surface properties, namely, the particle composition and collector adsorption (Albijanic et al., 2015). Once a particle collides with a bubble, it begins to slide over the bubble surface and resides there for a finite period. This period is generally referred to as the "sliding" time. Bubble-particle attachment should occur when the sliding time is longer than the induction time. The induction time is defined as the time required for the film thinning process.

It is generally recognized that the bubble-particle interaction is analogous to a chemical reaction. The particle must possess sufficient kinetic energy to overcome the energy barrier, which is created by the surface forces between the bubble and particle. As the particle overcomes the energy barrier, the disjoining film spontaneously ruptures, and adhesion occurs. This process is incorporated into an Arrhenius-type equation for P_a (Mao, 1998) as follows:

$$P_a = \exp\left(-\frac{E_1}{E_k}\right) \tag{12}$$

where E_1 is the energy barrier for bubble-particle adhesion, and E_k is the kinetic energy of collision. E_1 can be determined by the surface forces involved in the bubble-particle interaction that are described by the extended Derjaguin-Landau-Verwev-Overbeek (EDLVO) theory.

During flotation, the collision of bubbles and particles contribute to the kinetic energy of the system. Therefore, E_k is expressed as follows:

$$E_{\mathrm{k}} = \frac{(m_P \bar{V}_P'^2 + m_b \bar{V}_b'^2)}{2} \tag{13}$$

where m_{p} are m_{b} are masses of particle and bubble, respectively, $\bar{V}_p'$ and $\bar{V}_b'$ are mean fluctuating velocities of particle and bubble, respectively.

The density of the gas is negligible compared to that of the particle. Hence, the kinetic energy of bubble is ignored. The total kinetic energy E_{k} can be transformed into the following relationship:

$$E_{\mathrm{k}} \approx \frac{m_P \bar{V}_P'^2}{2} \tag{14}$$

Hence, Equations (13), and (14) can be used to derive P_{a} as follows:

$$P_a = \exp\left(-\frac{E_1}{E_{\mathrm{P}}}\right). \tag{15}$$

In a turbulent field, the kinetic energy of a particle with radius R_{P} is as follows:

$$E_P = \frac{1}{2} m_P \bar{V}_P'^2 = \frac{2}{3} \pi \rho_P R_P{}^3 \bar{V}_P'^2 \tag{16}$$

where ρ_{p} – particle density, Kg/m³.

Given the following:

$$\sqrt{\bar{V}_P'^2} = 0.33 \frac{\varepsilon^{4/9} d_P^{7/9}}{\nu^{1/3}} \left(\frac{\rho_P - \rho_f}{\rho_f}\right)^{2/3} \tag{17}$$

and substituting Eq. (17) into (16), the kinetic energy of particle can be expressed as follows:

$$E_P = 0.67 \frac{\varepsilon^{8/9} R_P{}^{41/9} \rho_P}{\nu^{2/3}} \left(\frac{\Delta\rho_P}{\rho_f}\right)^{4/3} \tag{18}$$

where ρ_{f} is a pulp density, kg/m^3 and $\Delta\rho_{\mathrm{p}} = \rho_{\mathrm{p}} - \rho_{\mathrm{f}}$, kg/m^3.

According to the extended DLVO theory, V is the sum of the repulsive electrostatic interaction energy (V_{E}), the attractive van der Waals interaction (dispersion) energy (V_{W}), and the hydrophobic interaction energy (V_{H}):

$$V = V_W + V_E + V_H. \tag{19}$$

(1) Van der Waals interaction energy

The influence of the flotation reagent adsorption layer is ignored. Hence, for the bubble and the particle with radii R_b and R_p, respectively, the V_E is given as follows:

$$V_W = -\frac{A_{132}}{6h} \cdot \frac{R_P R_b}{R_P + R_b} \tag{20}$$

where h is the distance between particle and bubble (m) and A_{132} is Hamaker constant, which characterizes the interaction between the particle and bubble in the aqueous solution:

$$A_{132} = A_{12} + A_{33} - A_{13} - A_{23} \tag{21}$$

$$A_{ij} \approx (A_{ii} A_{jj})^{1/2} \tag{22}$$

By substituting Eq. (22) into Eq. (21), we obtain:

$$A_{132} \approx (\sqrt{A_{11}} - \sqrt{A_{33}})(\sqrt{A_{22}} - \sqrt{A_{33}}) \tag{23}$$

where A_{11}, A_{22} and A_{33} refer to the Hamaker constants of the particle, bubble and aqueous solution, respectively, and $A_{11} = 6.07 \cdot 10^{-20}$ J, $A_{22} = 0$ J, and $A_{33} = 4.38 \cdot 10^{-20}$ J.

(2) Electrostatic interaction energy

The electrostatic force develops due to the interaction between the electrical double layers of the bubble and particle. The overlap between the double layers creates either attraction or repulsion, depending on their relative signs. If the bubble and the particle are considered as two spheres with radii R_b and R_p, respectively, then the expression for V_E is given as follows:

$$V_E = \pi \varepsilon_a \frac{R_P R_b}{R_P + R_b} (\psi_P^2 + \psi_b^2) \left(\frac{2\psi_P \psi_b}{\psi_P^2 + \psi_b^2} p + q \right) \tag{24}$$

P and Q are given by

$$p = \ln\left(\frac{1 + \exp(-kh)}{1 - \exp(-kh)}\right), \quad q = \ln(1 - \exp(-2kh)),$$

where:

– h is the closest distance between two surfaces;

– Ψ_p and Ψ_b are the surface potentials of the particle and bubble, respectively (mV); for flotation, Ψ_p =-0.017 V and Ψ_b =-0.030 V;

– ε_a is the absolute dielectric constant of the dispersion medium, $C^{-2}J^{-1}m^{-1}$, $\varepsilon_a = \varepsilon_0 \varepsilon_r$;

– ε_0 is the absolute dielectric constant of the vacuum, $8.854 \cdot 10^{-12}$ $C^{-2}J^{-1}m^{-1}$;
– ε_r is the dielectric constant of the dispersion medium; the ε_r for water is 78.5; and
– k the Debye reciprocal length, which represents the thickness of the electrical double layer and is mainly determined by the electrolyte concentration, nm.

The value of k is given by the following expression:

$$k = \sqrt{\frac{2e^2 N_A C Z^2}{\varepsilon_a K T}} \tag{25}$$

where
– K is the Boltzmann constant, $1.381 \cdot 10^{-23}$ $J \cdot K^{-1}mol$;
– T is the absolute temperature, K;
– e is the elementary charge, $1.062 \cdot 10^{-19}$ C;
– N_A is Avogadro's number, $6.022 \cdot 10^{23}$mol;
– C is the molar concentration of ions, mol/dm^3
– Z is ionic valence.

(3) Hydrophobic interaction energy

The hydrophobic interaction energy (V_H) is clearly attributed to the hydrophobic interaction between the surfactant and coated surfaces, and it decays exponentially with the separation distance (h) as follows:

$$U_H = -\frac{R_P R_b}{R_P + R_b} c h_0 k_1 \exp\left(-\frac{h}{h_0}\right) \tag{26}$$

where c is constant, $2.51 \cdot 10^{-3}$ $N \cdot m^{-1}$; h_0 is the decay length,10 nm; k_1 is the coefficient related to the particle surface contact angle, which can be expressed as follows:

$$k_1 = \frac{\exp\left(\frac{\theta}{100}\right) - 1}{e - 1} \tag{27}$$

Bubble-particle detachment

The combination of gravitational forces, turbulent forces and bubble oscillations acting on the attached particles are considered as attributes of detachment, which determine the upper limit of floating particle size. Probability of detachment P_d is higher for larger particles due to greater inertia. It also increases as the number of particles attached to the bubble surface increases.

A dimensionless Bond number *Bo´* can be defined as the ratio of the forces of detachment to the forces of attachment (Goel and Jameson, 2012). Thus, the following expressions can be derived:

$$P_d = \exp\left(1 - \frac{1}{Bo'}\right) \tag{28}$$

$$Bo' = \frac{4R_P^2[\Delta\rho_P g + 1.9\rho_P \varepsilon^{2/3}(R_P + R_b)^{-1/3}] + 3R_P\left(\frac{2\sigma}{R_b} - 2R_b\rho_f g\right)\sin^2\left(\pi - \frac{\theta}{2}\right)}{\left|6\sigma\sin\left(\pi - \frac{\theta}{2}\right)\sin\left(\pi + \frac{\theta}{2}\right)\right|} \tag{29}$$

Experimental

Apparatus

The structure and size charts of the flotation column are shown in Fig. 2. All of the size dimensions are in millimetres. The column heights and diameters are set to 650 and 100 mm, respectively. The height-to-diameter ratio is 6.5, which meets the requirements given by Yianatos (1989). The tailing device is not set. The circulating and aerating rates are adjusted using the pump outlet valve and the gas flow meter, respectively.

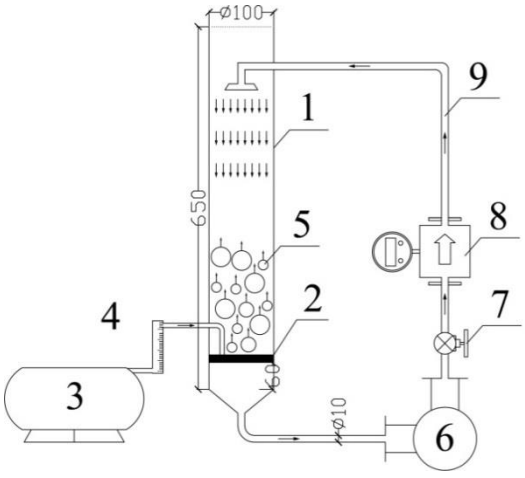

Fig. 2. Structure and size chart of the flotation column: (1) flotation column, (2) porous ceramic, (3) air compressor, (4) air flow meter, (5) bubble, (6) circulating pump, (7) valve, (8) water flow meter, and (9) circulating middlings

The bubble measurement system is set up based on the flotation column mentioned above. The bubble measurement system includes the bubble viewer, high-speed camera (i-SPEED 3, with the highest frame rate of 150,000 frames per second), image analysis system, light source (model DS-2000, power 168W), air flow meter (measurement range: 0.04~0.40 m^3/h), fluid flow meter (measurement range:

0.028~2.8 m^3/h, accuracy of 0.5), air compressor (FB-36/7 – revolving speed 1380 rpm, rated flow 102 dm^3/min, rated power 550 W), circulating pump (single phase vortex type self-priming pump – rated power 370 W, rated flow 1 m^3/h, rated head 18 m) and other ancillary equipments. The bubble measurement system is shown in Fig. 3.

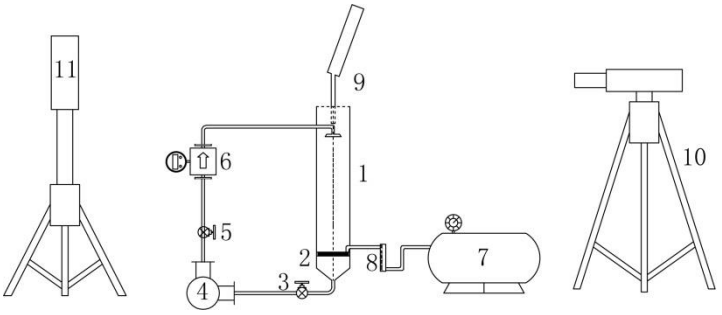

Fig. 3. Sketch map of a bubble measurement system: (1) flotation column, (2) porous ceramic, (3) valve, circulating pump, (5) valve, (6) water flow meter, (7) air compressor, (8) air flow meter, (9) bubble viewer, (10) high-speed camera, and (11) light source

Materials

To conveniently observe the bubble, the flotation column and the bubble viewer are constructed of glass. In the experiment, 2-octanol was used as afrother. 2-octanol is a branched C8 fatty alcohol and is directly produced from vegetal chemistry. This bio-based alcohol is manufactured through a cracking process from ricinoleic acid, a major component of castor oil.

In the calculation of the probabilities, the diameters of the particles were chosen as 10, 20, 30 and 45 μm. The bubble size was the actual measured value.

Methods

The experiments were conducted at temperature 25 °C. A principle diagram of bubble size measurements is shown in Fig. 4. Initially, 2-octanol was added to the deionized water of the column to prevent bubble coalescence (Li et al., 2013). The viewing chamber was then filled with the water-octanol solution to prevent bubble environment changes during sampling, and the tube was immersed into the appropriate location below the froth. The circulation pump was then turned on. After 2 min, air was introduced, and the airflow was adjusted by the rotameter and control valve. Bubbles raised into the viewing chamber and slid up toward the inclined window, and the light source illuminated these bubbles from behind. After 30 s, approximately 2000 pictures were obtained using the high-speed video camera. Finally, the bubble size d_{32} was calculated using DynamicStudio v3.20 image processing software (Wang, 2011).

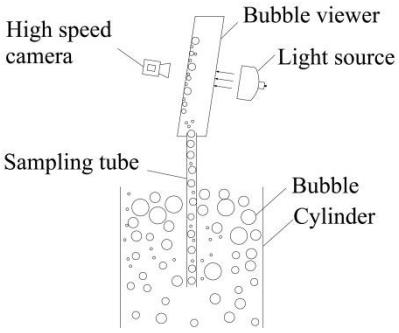

Fig. 4. Diagram for bubble size measurements

Results and discussion

The bubble diameters in the flotation column in different circulating volumes (0.253, 0.295, 0.342, 0.387, 0.413, 0.446, 0.467, and 0.495 m^3/h) are shown in Fig. 5. The bubble movement velocity is closely related to the bubble size, and the relationship between them is shown in Fig. 6.

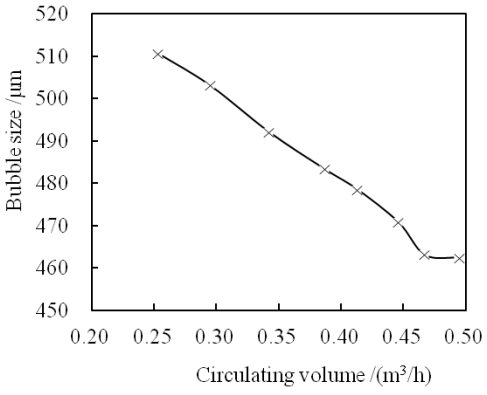

Fig. 5. The effect of circulating volume on bubble size

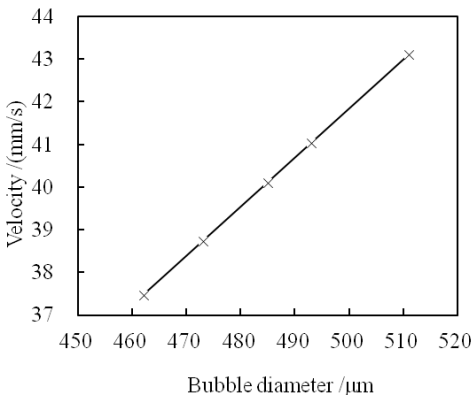

Fig. 6. The relationship between bubble diameter and velocity

Figure 5 shows that as the circulating volume increased, the bubble size decreased. A greater circulating volume results in a greater fluid turbulence intensity; therefore, the bubble size decreased. When the circulating volume increased from 0.253 to 0.495 m^3/h, the bubble diameter decreased from 511 to 462 μm.

Figure 6 shows that with increased bubble size, the bubble movement velocity increased. When the bubble diameter increased from 462 to 511 μm, the bubble movement velocity increased from 37.5 to 43.1 mm/s.

The computed results show that when the Reynolds number of the bubble was in the range of 17 to 22, the calculation of collision probability followed Eq. (10). The diameters of the chosen particles were 10, 20, 30 and 45 μm.

The collision probability of different circulating volumes in the countercurrent mineralization process is shown in Fig. 7. With increased particle size, the collision probability increased, and with increased circulating volume, the collision probability increased.

The turbulent kinetic energy of the particles was calculated using Eq. (17), and the results are shown in Fig. 8. Since the turbulent kinetic energy value was small, it was represented using a logarithmic scale. With increased particle size, the turbulent kinetic energy increased, and with increased circulating volume, the turbulent kinetic energy also increased. When the circulating volume increased from 0.253 to 0.495 m^3/h, for particles with diameters of 10 and 45 μm, the turbulent kinetic energy increased from $2.25 \cdot 10^{-21}$ to $5.72 \cdot 10^{-21}$ J and from $2.12 \cdot 10^{-18}$ to $5.41 \cdot 10^{-18}$ J, respectively.

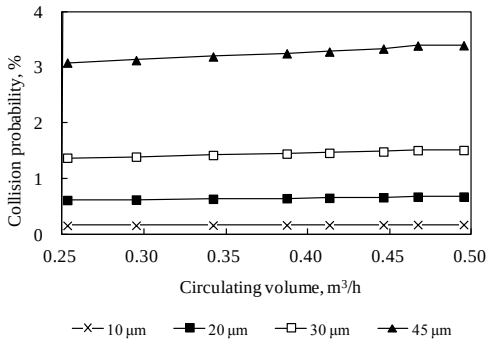

Fig. 7. The collision probability

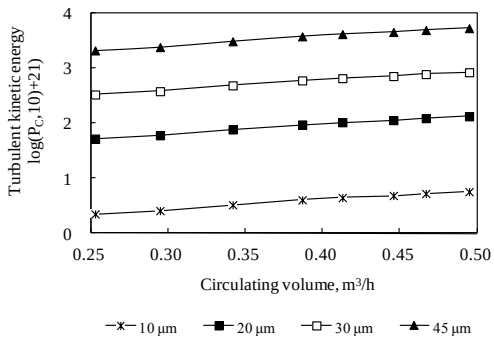

Fig. 8. The turbulent kinetic energy of particles

The relationship between the potential energy and distance in the bubble-particle interaction is shown in Fig. 9. The results showed that under the condition of the same circulating volume, as the particle size increased, the absolute value of the total potential energy between the particle and bubble increased. When the distance between the bubble and the particle was 30 nm, the energy barrier appeared. Only when the energy barrier was overcome could the attachment be realized. When the distance increased over 30 nm, the total potential energy was positive, and the value gradually approached 0. Under the condition of the same particle size, as the circulating volume increased, the absolute value of the total potential energy decreased. For particles with diameters of 10, 20, 30, and 45 μm, the energy barriers were $(4.92 \sim 4.93) \cdot 10^{-19}$, $(9.64 \sim 9.67) \cdot 10^{-19}$, 1.42×10^{-18}, and $(2.06 \sim 2.08) \cdot 10^{-18}$ J, respectively.

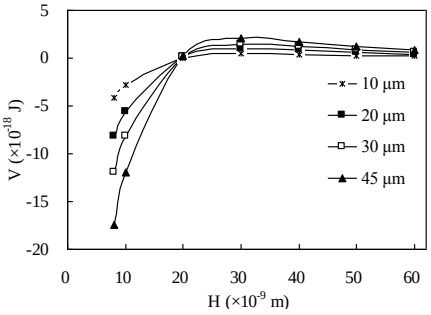

(a) 0.253 m^3/h

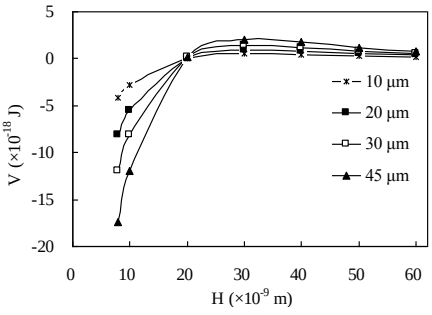

(b) 0.295 m^3/h

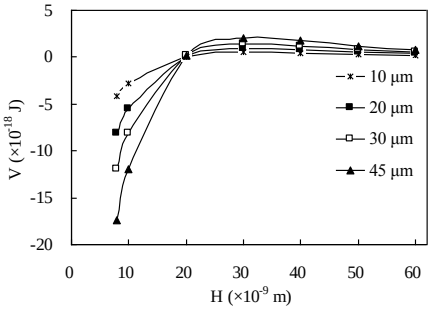

(c) 0.342 m^3/h

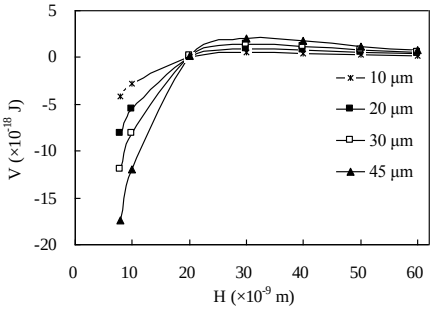

(d) 0.387 m^3/h

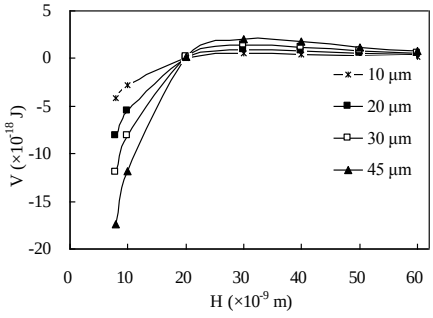

(e) 0.413 m^3/h

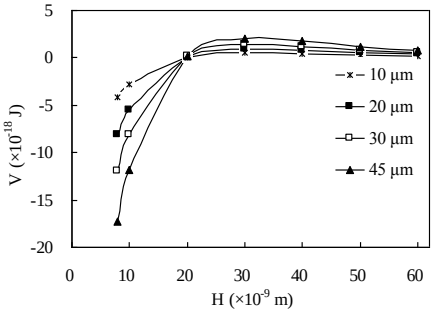

(f) 0.446 m^3/h

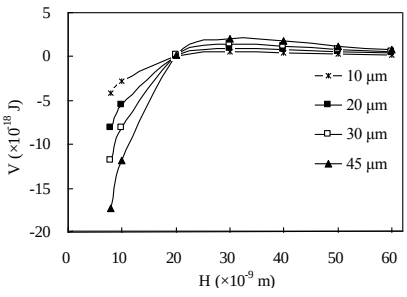

(g) 0.467 m^3/h

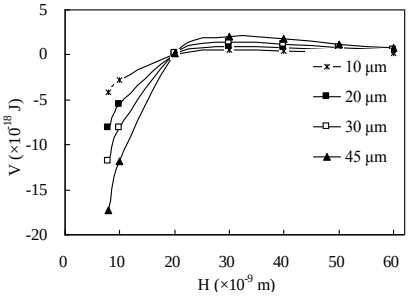

(h) 0.495 m^3/h

Fig. 9. The total interaction potential energy of particles and bubbles

The probabilities of attachment, detachment and acquisition between the particles and bubbles were calculated and are shown in Figs. 10, 11, and 12, respectively. As the particle size increased, the probabilities of attachment, detachment and acquisition increased, and as the circulating volume increased, the probabilities of attachment, detachment and acquisition increased. A greater circulating volume resulted in a greater turbulent kinetic energy of the particles, thus, a greater attachment probability. However, the increase in circulating volume increased the turbulence intensity and made it easier for the particle to detach from the bubble surface.

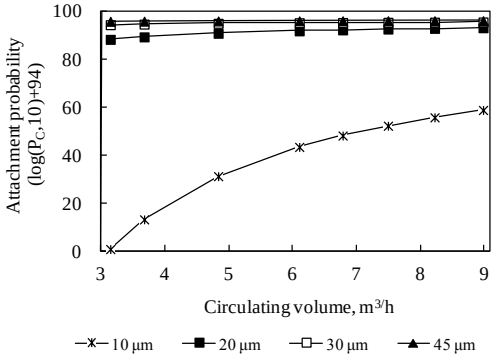

Fig. 10. Attachment probability

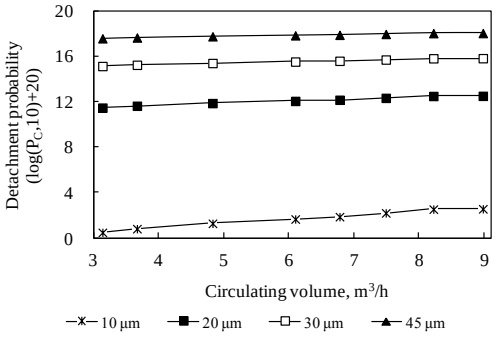

Fig. 11. Detachment probability

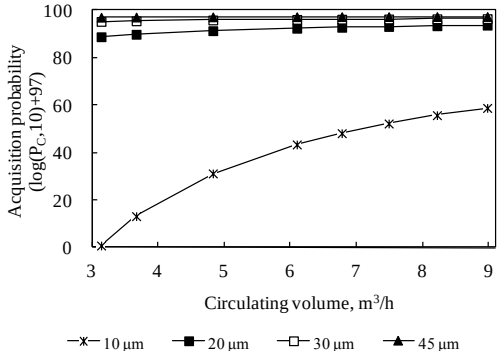

Fig. 12. Acquisition probability

Conclusions

Bubble-particle interactions play an important role in flotation. This paper presents considerable data supporting this finding. These results can be summarized as follows.

The bubble measurement system based on the flotation column was established. As the circulating volume increased, the bubble size decreased. The bubble velocity increased with increasing in bubble size. When the circulating volume increased from

0.253 to 0.495 m^3/h, the bubble diameter decreased from 511 to 462 μm, and the corresponding bubble velocity decreased from 43.1 to 37.5 mm/s.

Based on the above calculation of bubble size, the relationship between potential energy and distance in the bubble-particle interaction process was analysed. The results showed that under the condition of constant circulating volume, as the particle size increased, the absolute value of total potential energy between the particle and bubble increased. Under the condition of the constant particle size, as the circulating volume increased, the absolute value of the total potential energy decreased.

The probabilities of collision, attachment, detachment and acquisition between particles and bubbles were calculated. With increased particle size, the probabilities of collision, attachment, detachment and acquisition increased, and with increased circulating volume, the probabilities also increased.

Acknowledgements

The authors acknowledge the support from the Key Project of Science and Technology Research of Education Department of Henan Province (Grant No. 16A440002), Doctoral Foundation of Henan Polytechnic University (Grant No. B2015-13), National Key Basic Research Program of China (Grant No. 2012CB214905), and Beijing Natural Science Foundation (Grant No. 3154037).

References

ALBIJANIC B., NIMAL SUBASINGHEA G.K., BRADSHAWC D.J., NGUYENB A.V., 2015. *Influence of liberation on bubble-particle attachment time in flotation*. Miner. Eng., 74:156-162.

BASAOVÁ P., HUBIÇKA M., 2014. *The collision efficiency of small bubbles with large particles*. Miner. Eng., 66-68: 230-233.

DAI Z., FORNASIERO D., RALSTON J., 2000. *Particle-bubble collision models-a review*. Adv. Colloid Interface., 85 (2-3): 231-256.

EMERSON I.Z., 2007. *Particle and bubble interactions in flotation systems*. America: Auburn University, 2007: 22-23.

FIROUZI M., NGUYEN A.V., HASHEMABADIB S.H., 2011. *The effect of microhydrodynamics on bubble-particle collision interaction*. Miner. Eng., 24(9): 973-986.

FOSU S., SKINNER W., ZANIN M., 2015. *Detachment of coarse composite sphalerite particles from bubbles in flotation: Influence of xanthate collector type and concentration*. Miner. Eng., 71: 73-84.

GOEL S., JAMESON G. J., 2012. *Detachment of particles from bubbles in an agitated vessel*. Miner. Eng., 36-38: 324-330.

LI Y.F., ZHAO W.D., GUI X.H., ZHANG X.B., 2013. *Flotation kinetics and separation selectivity of coal size fractions*. Physicochem. Probl. Miner. Process. 49(2), 2013: 387−395.

MAO L.Q., 1998. *Application of extended DLVO Theory: Modeling of flotation and hydrophonocity of Dodecane*. America: Virginia Polytechnic Institute and State University: 24+45-48.

NGUYEN A.V., EVANS G.M., 2004. *Attachment interaction between air bubbles and particles in froth flotation*. Exp. Therm. Fluid Sci., 28 (5): 381-385.

NGUYEN A.V., SCHULZE H. J., 2004. *Colloidal Science of Flotation*. Marcel Dekker, New York: 840.

PYKE B., HE S.H., DUAN J.M., SKINNE W.M., FORNASIERO D., RALSTON J., 2004. *From turbulence and collision to attachment and detachment:general flotation model*. Proceedings of JKMRC International Student Conference, Hawaii: 77-89.

RAGAB S.A., FAYED H., 2012. *Collision frequency of particles and bubbles suspended in homogeneous isotropic turbulence*. AIAA Paper 2012-0310. AIAA 50th Aerospace Sciences Meeting, Nashville, TN, 9-12 January 2012.

RALSTON J., DUKHIN S.S., MISHCHUK N.A., 2002. *Wetting film stability and flotation kinetics*. Adv. Colloid Interface., 95 (2-3) : 145-236.

WANG H.Y., 2011. *Research on Image Processing Methods and Dynamic Characteristics of Bubble in Air-Water System*. Tianjin: Tientsin University, 1-100.

YIANATOS J. B., 1989. *Column Flotation Modelling and Technology*. International Colloquium: Developments in Froth Flotation. South Africa: Cape Town: 1-30.

YOON R.H., LUTTRELL G.H., 1989. *The effect of bubble size on fine Particle flotation*. Miner. Process. Extr. M., 5(l-4): 101-122.

ZHANG H.J., LIU J.T., WANG Y.T., CAO Y.J., MA Z.L., LI X.B., 2013. *Cyclonic-static micro-bubble flotation column*. Miner. Eng., 45: 1-3.